Augmentation of the Slow-Time k-Space for Narrowband High-Resolution Radar Imaging

Hai-Tan Tran[1], Emma Heading[1,2], and Brian Ng[2]
[1] 180 Labs, National Security and ISR Division, DST Group
Third Ave, Edinburgh SA, 5111, AUSTRALIA
[2] School of Electrical Engineering, University of Adelaide,
Adelaide, SA, 5000, AUSTRALIA

haitan.tran@dst.defence.gov.au

ABSTRACT

High resolution imaging with a narrowband radar offers a promising technology response to the challenge of electromagnetic spectrum congestion in which radar operation is losing more and more of the allocated spectrum to mobile communication networks. In this solution space, radar tomography, which exploits the spatial diversity of a system, is a key signal processing paradigm. Doppler radar tomography (DRT) is a special form of radar tomography where Doppler processing on a single-frequency (or ultra-narrowband) signal provides a simple yet critical tool for cross ranging; this work takes DRT to the next level, in the context of the slow-time k-space.

The slow-time k-space is a novel form of the spatial frequency space generated by the relative rotational motion of a target, at a single radar frequency; such a space can be exploited for high-resolution target imaging by a narrowband radar. The paper presents a brief theory of the slow-time k-space in the context of Doppler tomography, describes its useful characteristics of augmentability for wider supports; the wider a k-space support, the higher the resulting image resolution.

Well-known techniques in compressive sensing, such as orthogonal matching pursuit (OMP), can be efficiently used for the augmentation of a slow-time k-space. Assuming that any translational (bulk) motion is well compensated prior to this processing, the dictionary we use with OMP processing consists of simple quadratic chirp functions which can model the rotational motion of a target. The parameter space defining the dictionary is thus limited to two dimensions, allowing a manageable size of the dictionary and hence reasonable computational cost.

The paper describes a demonstration of the OMP-based slow-time k-space augmentation using experimental radar data. Phenomena associated with electromagnetic scattering in real targets, such as 'creeping waves', are observed and discussed in relation to this proposed technique. Other possible applications are also briefly mentioned.

1.0 INTRODUCTION

Tomography is a general imaging technique that is based on lower-dimensional measurements or projections of an object at a range of different spatial aspects, which are then processed using the projection-slice theorem [1] to reconstruct an image of the object. Radar tomography uses reflective scattering phenomenology and radar waveforms for the measurements, which may be wideband or narrowband. Wideband waveforms represent spectral diversity – one of the system resources for radar imaging and probably the most exploited resource in practical applications in the last few decades. The well-known synthetic aperture radar (SAR) and inverse SAR (ISAR) imaging techniques may be described as two special forms of wideband tomography, in which another system resource – spatial diversity – is exploited only minimally [2]. Range-Doppler ISAR imaging and stripmap SAR in particular typically involve aspect angle

changes of a few degrees [3–5]. This constraint to small rotation angles in the linear phase regimes allows the image inversion processing to take advantage of the computationally efficient fast Fourier transform (FFT), and to avoid the need for signal interpolation onto rectangular grids.

Spotlight SAR makes use of wider angles [6,7], while circular SAR [8] may coherently process up to a complete cycle of target aspect rotation, with sophisticated and precise motion compensation in the range dimension. More notably, in the associated spatial frequency spaces, also known as *k*-spaces [2], traditionally intensive interpolation processing prior to image inversion processing may be necessary. Nevertheless, these forms of SAR and ISAR may be described as belonging to the category of 'wideband radar tomography'.

Radar tomographic imaging with ultra-narrowband or single-frequency waveforms relies on spatial diversity as the only system resource for image formation. Spatial diversity may be realized by: (i) having a radar with multiple receivers looking at the target from diverse angular locations, the received signals from which are processed coherently, or (ii) using a single receiver looking at a target undergoing relative rotational motion, i.e. changing target aspect. Both cases widen the angular extents of the measurement support of the received signal in the associated *k*-spaces.

As discussed in [2], narrowband radar tomography can be most effectively formulated in the *slow-time k*-space in conjunction with the classical Doppler processing and Doppler radar tomography (DRT) [9,10]. The DRT algorithm applies the projection-slice theorem in which the inputs as target's cross-range projections are formed from Doppler profiles. The slow-time *k*-space is not only convenient for describing the DRT algorithm, it is also a natural tool to formulate high-resolution DRT imaging with an augmentation of its measurement support. How *k*-space augmentation may be achieved is the subject of the current work; it is sufficient to mention briefly here that augmentation is the process of significantly enlarging the support of the slow-time *k*-space by using longer CPIs in the DRT algorithm and correcting for nonlinear phase effects due to strong rotational motion. This 'augmentability' is a unique characteristics of the slow-time *k*-space.

Slow-time *k*-space augmentation can be achieved by a combination of the more traditional techniques of fractional Fourier transform and the S-method, as described in [10]; the current work extends to the more modern technique of orthogonal matching pursuit (OMP) of compressive sensing. The main contribution of the paper is two-fold: to highlight the augmentability of the slow-time *k*-space as a key characteristic for narrowband radar imaging, and to present a novel application of the OMP technique to such augmentation processing.

The rest of paper is organized as follows. The next Section summarizes the fundamental theory: system geometry and signal model, cross-range bandwidth and resolution, and DRT. Section III describes the slow-time *k*-space and its augmentation with OMP processing. Section IV describes an experimental setup and imaging results for both standard and augmented DRT processing. The final Section presents some relevant discussion points and concluding remarks.

2.0 BACKGROUND

This Section defines the signal model and summarizes the known theory of Doppler radar tomography (DRT).

2.1 Signal Model

We assume the usual point-scatterer target model; a typical system geometry is illustrated in Fig.1, with a monostatic radar illuminating a target. As usual in target imaging literature, an inertial local target reference frame, denoted as $\boldsymbol{T}_x$ with origin at the target's nominal centre of rotation, can be chosen to have the x axis being the cross-range axis, while the y axis (the 'down-range axis') aligned with the radar line of sight

(LOS). The plane (*x*, *y*) is sometimes known as the image projection plane (the IPP, or simply 'image plane'). The third axis for 'height', *z*, is orthogonal to the image plane and points along the target's effective rotation vector $\boldsymbol{\Omega}_e$ which is a component of the target's total rotational velocity vector $\boldsymbol{\Omega}$ along this axis.

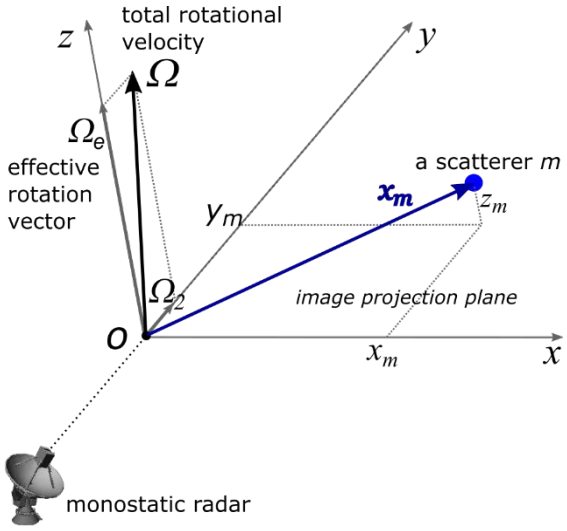

Figure 1: Imaging system geometry: The (x, y, z) coordinates define the local target frame, T_x. Only one scatterer of the target is shown at x_m, which rotates around origin O with velocity Ω.

By definition of $\boldsymbol{T}_x$,

$$\boldsymbol{\Omega} = (0, \Omega_2, \Omega_e), \tag{1}$$

Component Ω_2 has no contribution to radar imaging, while Ω_e is what makes motion-based target imaging possible. Both of these components and the orientation of the IPP itself, are generally unknown a priori. In this paper, we restrict our consideration to target imaging in 2D only, and hence will assume further that $\Omega_2 = 0$, and Ω_e is at least approximately constant during a coherent processing interval (CPI).

A point-scatterer assumption means the target may be modelled as an ensemble of M point scatterers with reflectivity coefficients σ_m located in the far field of the radar. The range to the m^{th} point-scatterer on the target with position vector $\boldsymbol{x}_m$, defined relative to O, can be approximated as

$$R(\boldsymbol{x}_m) \approx \boldsymbol{R}(\boldsymbol{x}_m) \cdot \boldsymbol{i}_{LOS} = R_0 + r_m\,, \tag{2}$$

in which $\boldsymbol{R}(\boldsymbol{x}_m)$ is the range vector to the m^{th} scatterer, R_0 is the radar range to O, local scatterer down range is

$$r_m = \boldsymbol{x}_m \cdot \boldsymbol{i}_{LOS}\,, \tag{3}$$

And $\boldsymbol{i}_{LOS}$ is the unit vector along the radar LOS. Specifically, $\boldsymbol{i}_{LOS} = (0, 1, 0)$ in the $\boldsymbol{T}_x$ frame.

The $\boldsymbol{T}_x$ frame is convenient for describing a target's rotational motion, and has been used in traditional (small angle) ISAR imaging formulation. For radar tomography which exploits spatial diversity through wide changes of target aspect, a similar local target frame, here denoted as $\boldsymbol{T}_y$, is more convenient. This frame is fixed with the target and shares the same x_3-axis with $\boldsymbol{T}_x$; the two frames coincide only at a reference time $t_k = 0$. The $\boldsymbol{T}_y$ frame is convenient because its axes are aligned with those of the underlying

k-spaces; angles are also preserved across the $\boldsymbol{T}_y$ frame and the *k*-spaces, as will become evident in the following.

Let $s_T(t_k;f) \propto \exp\{j2\pi f t_k\}$ denote the simple transmit continuous waveform at a single frequency *f*, where only the slow time t_k is involved; there are no pulses and hence no 'fast time' spanning a pulse. The slow-time index is $k = 0,1,2,\dots,K-1$, and we assume a total of *K* time samples in a CPI. The receive signal $s_R(t_k;f)$ is modelled as a delayed version of $s_T(t_k;f)$,

$$s_R(t_k,f) \propto \exp\left\{-j4\pi f \frac{R_0(t_k)}{c}\right\} \sum_{m=1}^{M} \sigma_m \exp\left\{-j\frac{4\pi f}{c} r_m(t_k)\right\}. \tag{4}$$

Here, we assume that quadrature down-conversion processing is perfectly accomplished by radar hardware; the carrier term has also been removed. The first factor in (4) accounts for translational motion; the second factor captures the target geometry and scattering reflectivities to be processed for imaging.

Furthermore, we shall assume a linear translational motion model for the target, i.e.

$$R_0(t_k) = R_{init} + v\, t_k\,, \tag{5}$$

where v is the velocity, assumed known prior to DRT processing, and R_{init} is target range at a reference time $t_k = 0$.

2.2 Cross-Range Bandwidth and Resolution

Relative to $\boldsymbol{T}_x$, the local down range r_m in (4) can be explicitly expressed, to the second order in slow time, as

$$r_m(t_k) = y_m + x_m \Omega_e t_k - \frac{1}{2} y_m \Omega_e^2 t_k^2 + \cdots, \tag{6}$$

Here, x_m, y_m are the cross range and range of a scatterer with index *m* in $\boldsymbol{T}_x$ at the reference time $(t_k = 0)$ of the CPI with duration T_{CPI}. As has been thoroughly discussed in [2], although y cannot be directly estimated with a zero-bandwith signal, the *first*-order term of (6) suggests that a *cross-range bandwidth*,

$$B_\perp = f\, \Omega_e T_{CPI} = f\, \Delta\theta\,, \tag{7}$$

may be defined, which can be used to estimate cross range x. Target rotation thus generates an effective bandwidth for the cross-range dimension, as long as T_{CPI} , or more precisely the rotation angle $\Delta\theta = \Omega\, T_{CPI}$ is sufficiently small such that the first-order approximation of (6) is valid. This puts a stringent constraint on $\Delta\theta$ of a few degrees, which is a common requirement in ISAR imaging, and hence a relatively small $B_\perp$. Furthermore, the presence of the zeroth-order term y, which is generally unknown at this stage, prevents an estimation of x directly from the time-domain signal. Nevertheless, Doppler tomography can be used to overcome the constraints and challenges.

By performing a standard Fourier transform (over t_k) on a segmented CPI of the narrowband receive signal $s_R(t_k,l)$, a Doppler profile $S_R(f_d) = \mathcal{F}\{s_R(t_k,l)\}$ can be formed, where zero Doppler ($f_d = 0$) corresponds to the centre of rotation at *O* (again assuming perfect translational motion compensation had been applied prior to this processing), and the associated Doppler resolution is

$$\Delta f_d = \frac{1}{T_{CPI}} = \frac{f\Omega_e}{B_\perp}. \tag{8}$$

All scatterers over the available range of y are 'collapsed' ('projected') onto the Doppler profile. Since the instantaneous cross-range of a scatterer is directly proportional to its (monostatic) Doppler frequency f_d, namely

$$x = \frac{\lambda}{2\Omega_e} f_d\,, \tag{9}$$

the *magnitude* of the Doppler profile, $p_\theta(x) = |S_R(f_d)|$, with θ denoting the (average) aspect angle for this CPI, represents a cross-range projection of the target's reflectivity function. Taking a differential of (9), i.e. $\Delta x = (\lambda/2\Omega_e)\,\Delta f_d$, and using (8), we obtain a *cross-range resolution* of

$$\Delta x = \frac{c}{2B_\perp}. \tag{10}$$

This is the same form that (down) range resolution Δy is conventionally expressed in terms of spectral bandwidth *B*: $\Delta y = c/2\mathrm{B}$.

2.3 Doppler Radar Tomography

Once the required cross-range profiles are formed, the fundamental 'Projection-Slice Theorem' (PST) of radar tomography can be used for image formation, i.e. to estimate both x and y of all scatterers present in the signal. According to the PST, the Fourier transform $P_\theta(f_{s\perp})$ of projection $p_\theta(x)$ is a slice of the 2D FT of the target function at aspect angle θ; by computing these 1D cross-range projections and assembling them in the frequency domain over sufficient extent of the target's aspect, its reflectivity function (the target image) can be reconstructed by a standard 2D inverse FT operation.

2.3.1 The Monostatic DRT Algorithm

In practical applications, the algorithm to populate the support of the slow-time k-space is illustrated in Fig.2, which consists of the following steps:

1. *Data segmentation*: the set of all *N* samples $s_R(t_n)$ in the received data block is segmented into *L* overlapping CPIs, $s_R(t_k, l)$, each of length *K* samples and with an overlap factor η. These CPIs are also called 'segmented CPIs'. Here, $K = 0,1,\dots,K;\ \ l = 1,2,\dots,L;$ and $0 \le \eta \le 1$. The target aspect angle (relative to $\boldsymbol{T}_x$) at the mid-point of such a segment is denoted as θ_l ;

2. *Translational motion compensation (TMC)*: this is applied to each CPI, by multiplying the signal with a linear phase factor $\exp(j2\pi v t_k)$, to shift the Doppler line of known non-rotating components to zero Doppler frequency. Here, v is the target's translational velocity as noted in (5), assumed to be known or estimated by other methods. A standard Fourier transform is then applied to all segments, with a circular shift to place the zero Doppler frequency at the centre of the spectrum. Denote the magnitude of the output as

$$p_\theta(x_1) = |\mathcal{F}\{s_R(t_k, l)\exp(j2\pi v t_k)\}| \tag{11}$$

for the cross-range profiles. Accumulate all such cross-range profiles, along with the corresponding aspect angles θ_l, available from the data block.

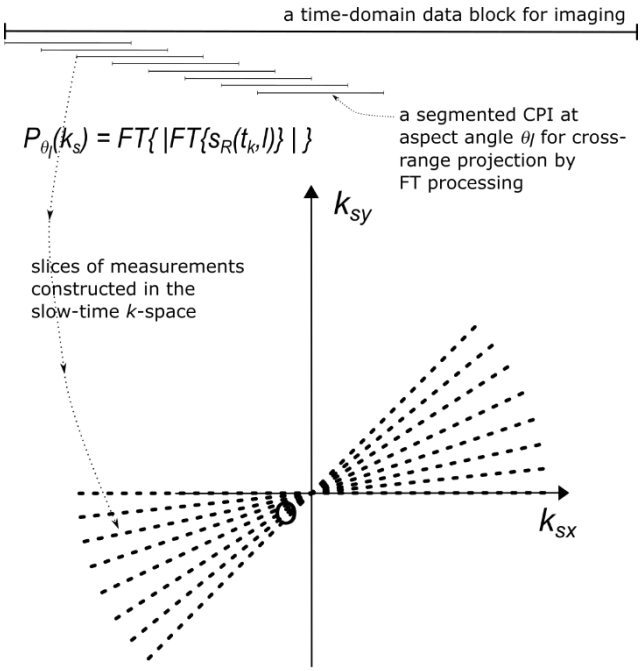

Figure 2: An illustration of the algorithm for Doppler radar tomographic (DRT) imaging using the slow-time *k*-space. The k_{sy}- and k_{sx} axes describe components of k_s as defined in (15)

3. *Populating the k-space*: The spatial Fourier transform of $p_\theta(x)$, namely

$$P_{\theta_l}(f_{s\perp}) = \mathcal{F}\{p_{\theta_l}(x)\} \tag{12}$$

are then used as the 'measurement samples' at aspect angle θ_l to populate the slow-time *k*-space. As the target rotates, the measurements 'fan out' as indicated in Fig.2. Note that the measurement population always starts close to the k_{sx}-axis because $p_{\theta_l}(x)$ are cross-range profiles.

4. *Image inversion*: The populated support of the *k*-space is applied to an inverse Fourier transform to yield the target image. Traditionally, the filtered back projection, or an interpolation onto a rectangular grid followed by a 2D inverse Fourier transform, could be applied [9], [10]. Here, we shall make use of the non-uniform Fast Fourier transform (NUFFT).

2.3.2 Standard DRT

'Standard DRT' refers to the case where the input cross-range profiles, as mathematically defined by (11), are Doppler migration free (DMF) free, and the rotation angle corresponding to each profile is within the linear limit. The DMF condition can be satisfied when the segmented CPI lengths are sufficiently short such that the nonlinear phase terms in (6) are negligible and hence compensation is not necessary, or when $|\boldsymbol{x}_m|$ is small. The former case is particularly sensitive for scatterers at larger radial distances from the centre of rotation, while the latter case applies more to scatterers sufficiently close to the centre of rotation whose Doppler frequencies are small and Doppler migration effects (if any) are also small.

As derived in [11], the standard DRT constraints on CPI rotation angle is

$$\Delta\theta \leq \min\{\Delta\theta_{DM}, \Delta\theta_{LM}\}\ ,\ \ (\text{rad}) \tag{13}$$

where $\Delta\theta_{DM} = (\lambda/2r_{max})^{1/2}$ is an effective rotation angle required to induce a Doppler migration (DM) of

one bin, $\Delta\theta_{LM}$ is the 'linear limit', while DRT image resolution, in both range and cross range, is

$$\Delta x = \Delta y \geq \left(\frac{\lambda\, r_{max}}{2}\right)^{1/2} . \quad \text{(m)} \tag{14}$$

Here, r_{max} is the maximum radial dimension of the target. Note that $\Delta\theta$ and Δx are independent of rotation rate and signal sampling rate, but only on radar wavelength and the dimension of the target (through maximum radial dimension r_{max} to any scatterer). $\Delta\theta_{LM}$ is roughly 10 degrees; equations (13) and (14) can be used as a guide to predict the expected imaging performance or applicability of standard DRT for a specific radar wavelength and target size.

'*Augmented DRT*' involves wider rotation angles and processing to compensate for nonlinear effects due to rotation, as discussed in the next Section.

3.0 THE SLOW-TIME K-SPACE AND ITS AUGMENTATION

While it is possible to formulate the problem and solution entirely in terms of the spatial frequency space of $f_{s\perp}$, we shall keep up with tradition and formulate it in terms of a '*k*-space', with $k_s = 2\pi\, f_{s\perp}$.

3.1 The Slow-Time *k*-Space

In basic Fourier analysis, for signal with a pulse repetition interval PRI, the Doppler frequency extent of the signal is $PRF = 1/PRI$, which spans the interval $(-PRF/2, PRF/2)$. Analogously, from the spatial (cross-range) resolution Δx as given in (10), the extent of spatial frequency $f_{s\perp}$ is $1/\Delta x = 2B_\perp/c$, which symmetrically spans the interval $(-B_\perp/c, B_\perp/c)$. Making use of (7), the interval for k_s is thus

$$k_s \in \left(-\frac{2\pi f}{c}\Delta\theta, \frac{2\pi f}{c}\Delta\theta\right),$$

as illustrated by the radial dashed lines in Fig.2. When forming the cross-range profile with the computationally efficient FFT, the number of samples in time domain and frequency domain are equal, to *K*. Hence, the (discretized) slow-time *k*-vectors $\boldsymbol{k_s}$ corresponding to each cross-range projection can be defined as

$$\boldsymbol{k_s} = k'\frac{2\pi f}{c}(\Omega_e T_{PRI})\, \boldsymbol{i}_\perp , \tag{15}$$

where $k' = -K, -K+2, \ldots, -2, 0, 2, \ldots, K-2; T_{PRI} = T_{CPI}/K,$ and $\boldsymbol{i}_\perp$ is the cross-range unit vector (perpendicular to $\boldsymbol{i}_{LOS}$) along the x-axis of the $\boldsymbol{T}_x$ frame.

The slow-time *k*-space arises naturally out of DRT: its *support* (radial extent) is determined by the cross-range bandwidth $B_\perp$ and its *populating samples* are $P_{\theta_l}(k_s)$ given by (12); as the target rotates, the slow-time *k*-space support is swept out in fan-like shapes around the *k*-space origin. Also, for a given $B_\perp$, the number of $\boldsymbol{k_s}$ points is a processing design parameter not necessarily fixed to *K*; its chosen value however would affect only the sidelobes of the impulse response, and hence image contrast, not image resolution.

An important and useful characteristics of the slow-time k-space is it can be augmented. As implied by (7), $B_\perp$ can be increased by using a wider rotation angle $\Delta\theta$, at the cost of further processing to correct for the nonlinear terms in the phase function of (6). In Section III-B below, we discuss one typical technique to correct for the *second*-order term, i.e. linear chirp components; augmentation of the *k*-space is enabled by

using wider segmented CPIs such that linear chirps are sufficient to model the rotational motion of all point scatterers.

Let us define an 'augmentation factor' as

$$\kappa = \frac{\Delta\theta}{\Delta\theta^{(s)}} = \frac{T_{CPI}}{T_{CPI}^{(s)}}\,, \tag{16}$$

where $T_{CPI}^{(s)}$ and $\Delta\theta^{(s)}$ denote the standard segmented CPI length and the corresponding rotation angle in the conventional linear limit of narrowband imaging. Then, according to (7) and (15), the cross-range bandwidth $B_{\perp}$, the radius of the slow-time *k*-space, and hence DRT image resolution, will all be increased by a factor of κ. The augmentation of the slow-time *k*-space is conceptually illustrated in Fig.3. The DRT algorithm based on an augmented *k*-space is called augmented DRT.

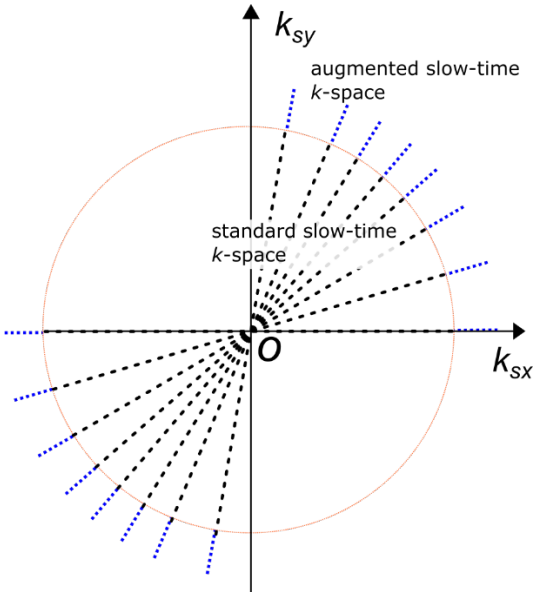

Figure 3: A conceptual illustration of the augmentation of the slow-time *k*-space. The circle indicates the boundary of support in standard DRT imaging.

3.2 Augmented DRT with Orthogonal Matching Pursuit (OMP)

This technique shares the same objective as the technique based on the fractional Fourier transform and S-method, as reported in [10], but instead makes use of a popular tool in the more modern approach of sparse signal reconstruction: OMP. Again, TMC is assumed to have been perfectly processed prior to this processing.

3.2.1 Sparse Representation

With reference to (4) and (6), the segmented CPI signal is represented in vector form as

$$\boldsymbol{s}_R = \boldsymbol{\Psi}\boldsymbol{\sigma} + \boldsymbol{\epsilon}\,, \tag{17}$$

where $\boldsymbol{\Psi}$ is the dictionary matrix of size $K \times N_\sigma$; $\boldsymbol{\sigma}$ is a length-N_σ column vector of (complex-valued) atom coefficients; and $\boldsymbol{\epsilon}$ is a length-*K* column vector of noise and/or clutter components. The columns of are the

chirp atoms, of the form

$$g(k) = \exp\left\{-j2\pi\left(f_g t_k + \tfrac{1}{2} c_g\, t_k^2\right)\right\}, \tag{18}$$

where $k = 0,1,\ldots,K-1$, and the parameters

$$f_g = \frac{2\,x\,\Omega_e}{\lambda}, \qquad c_g = \frac{2\,y\,\Omega_e^2}{\lambda} \tag{19}$$

respectively represent the Doppler frequency and chirp rate of a scatterer due to rotation, at reference time $t_k = 0$, which define the atom $g(k)$. Furthermore, let f_g and c_g, or equivalently x and y, be uniformly discretized by two vectors of expected or possible values, of lengths N_f and N_c respectively, then $N_\sigma = N_f N_c$.

The OMP algorithm itself is well-known (see [12] for example), is one of several sparse reconstruction techniques that could be used in this algorithm.

3.2.2 The OMP-Based Augmented DRT Algorithm

The augmented DRT algorithm is modified from standard DRT by simply lengthening the segmented (and overlapping) CPIs with an augmentation factor κ, as defined by (16); the target signal in each CPI can then be represented as a sum of linear chirp components. The aim is then to estimate such a representation and to correct for the chirps, i.e. focusing the range profile, before applying them to remaining steps of the DRT algorithm. OMP is one possible approach for this purpose.

For each augmented CPI, suppose the output of the OMP processing is a (sparse) solution support $\left\{f_g^{(m)}, c_g^{(m)}\right\}$ of size *M* with corresponding atoms $\{g_m(t_k)\}$ and coefficients $\{\sigma_m\}$, then a *dechirped* version for the segmented receive signal is

$$\tilde{s}_R(t_k) = \sum_{m=1}^{M} \sigma_m\, g_m(t_k) \;\Rightarrow \sum_{m=1}^{M} \sigma_m\, \tilde{g}_m(t_k)\,. \tag{20}$$

The right arrow $\Rightarrow$ above denotes a *replacement* of the $g_m(t_k)$ atom with a corresponding *single-tone* function

$$\tilde{g}_m(t_k) = \exp\left\{-j2\pi f_g^{(mid)} t_k\right\}, \tag{21}$$

with Doppler frequency

$$f_g^{(mid)} = f_g^{(m)} + \frac{1}{2} c_g^{(m)}\, t_{mid}\,, \tag{22}$$

so defined as the instantaneous frequency at t_{mid} – the middle time of the segmented CPI. The operation

$$p_{\theta_l}(x) = \left|\mathcal{F}\{\tilde{s}_R(t_k)\}\right| \tag{23}$$

then would give a focused cross-range projection for tomographic processing. The replacement of a chirp atom with a pure-tone atom at an appropriate time removes the usual spread in Doppler processing, hence the

focusing effect.

The augmentation algorithm, applied to each CPI of the augmented DRT algorithm, can thus be summarized as follows.

0. *Initialize*:
    a. define or select expected intervals of Doppler frequency f_g and chirp rate c_g;
    b. define the corresponding chirp atoms and set up the dictionary $\boldsymbol{\Psi}$;
    c. input segmented CPI data $s(t_k)$;
1. Compute the OMP-based sparse representation;
2. Replace all chirp atoms in the sparse solution with single-tone sinusoid functions with Doppler frequency at the mid-point of the segmented CPI;
3. Compute the focused cross-range profile p_{θ_l} as given by (23).

4.0 EXPERIMENTAL RESULTS

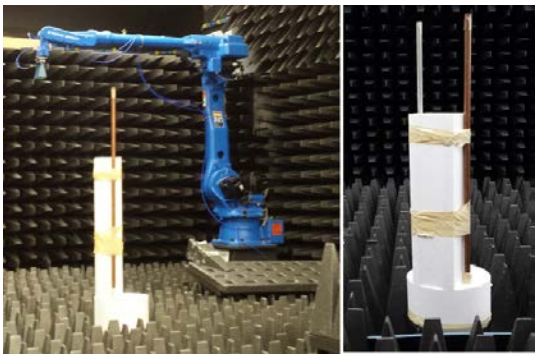

Figure 4: An example of an antenna mounted on a robotic arm at the Mumma Radar Laboratory with the two vertical metallic rods secured to the rotating pedestal.

4.1 Experimental Setup

The datasets used in this work were collected in the Mumma Radar Laboratory at the University of Dayton, Ohio, USA. Although the aim of the study is narrowband imaging, a wideband waveform at X-band was used with stepped-frequency pulses between 8 GHz and 12 GHz, over 101 regular frequency steps. Only the measured data from one of the available discrete frequencies f_k was used to study narrowband tomographic radar imaging.

The transmit and receive horn antennas were mounted on separate robotic arms which could be oriented and positioned with high precision. The measurements were conducted in a controlled laboratory environment with some radar absorbing material (RAM) reducing the radar reflections from the floor and walls. The experimental target consisted of two vertical metallic rods, separated by 19 cm (approximately), emulating two point scatterers which rotated around a vertical pedestal, as illustrated in Figure 4. The maximum radial distance is 11 cm. The antennas were kept stationary whilst the target was rotated through 360 degrees, at 0.1-degree steps. At each angular step, the stepped-frequency waveform was transmitted and sampled, one sample for each frequency.

4.2 Emulation of a Rotating Target

Target rotational motion, radar sampling rate, and other key signal processing parameters can be emulated from the stop-start measurements described above. While full theoretical details are explained in [11], the steps for the emulation may be described in the following.

- f_k: we choose the lowest and highest frequencies available in this experiment, 8 and 12 GHz, corresponding to $\lambda = 3.75$ or 2.5 cm. With $r_{max} = 0.11$ m, $\Delta\theta_{DM} = 23.7$ deg or 19.3 deg respectively. We also choose $\Delta\theta_{LM} = 10$ deg; the system is thus $\Delta\theta_{LM}$-limited and poor imaging performance can be expected from standard DRT;
- The condition for Doppler ambiguity free is $PRF > 4\omega r_{max}/\lambda$; *PRF* should be designed such that $PRF_a = PRF/\omega$ – the angular sampling rate (in samp/rad) – is greater than $4r_{max}/\lambda$ = 11.7 or 17.6 by a factor as close to 1 as possible, which could ease hardware sampling rate requirement.
- The angular sampling interval of 0.1 degree per sample in the experiment translates to a $PRF_a = 573$ samp/rad. Over the chosen $\Delta\theta_{LM}$ value, 100 samples are available. To reduce computational cost while retaining a reasonable FFT length and satisfying the Doppler ambiguity free condition, we use a down sampling ratio of 3:1, leading to *K* = 33 samples per CPI, and $PRF_a = 1911$ (samp/rad). This choice also satisfies the constraints of Doppler migration free of standard DRT and linear phase limits.

Realistic values for *PRF* and ω can also be chosen such that PRF/ω = 191; this is however not necessary, and all essential parameters of the emulated system are set up for DRT processing.

For each of the selected frequencies, an elliptic filter with a very narrow stop band is also applied to the signal as a pre-processing for clutter removal. Results are shown in Sections 4.3 and 4.4.

4.3 Standard DRT Imaging

To demonstrate *k*-space augmentation and the usefulness of sparse signal reconstruction, some typical results of standard DRT imaging is now shown. For the emulated system described above, Figure 5 shows a spectrogram of the signal at 8 GHz. The small value of $4r_{max}/\lambda$ compared to PRF_a causes the target Doppler content to be confined to approximately only 9 of the 33 Doppler bins available. Figure 6 shows the corresponding slow-time *k*-space support and standard DRT image. We have used an overlapping factor η of 0.99 in the segmentation step to provide a very smooth angular coverage of the *k*-space. However, the *k*-space support is small, and as expected, standard DRT imaging performance is poor; there are not enough resolving pixels on the two scatterers (the metallic rods) for a clearer image.

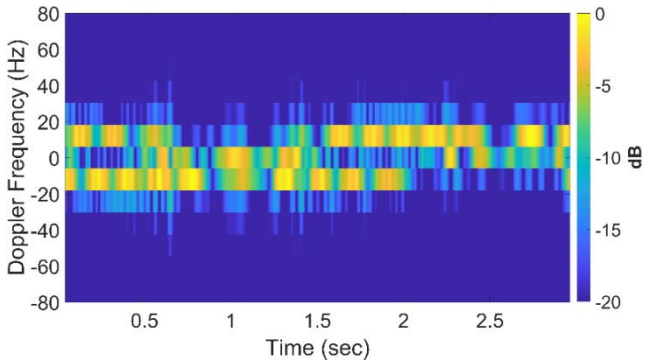

Figure 5: Spectrogram of emulated signal, standard DRT, for *f* = 8 GHz

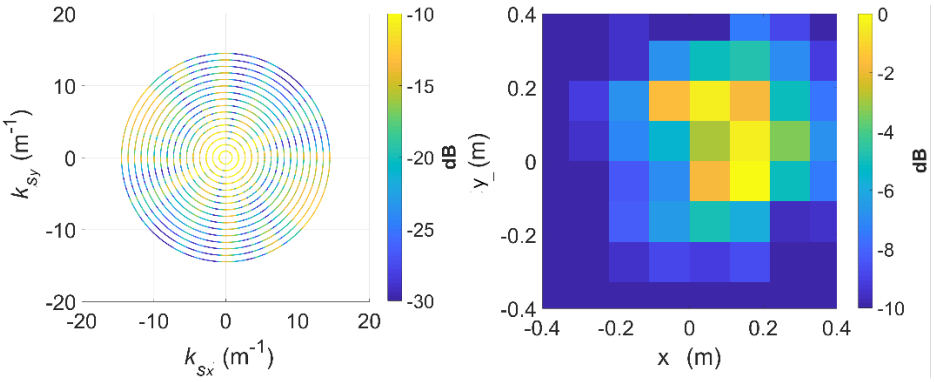

Figure 6: The slow-time *k*-space support (left) and corresponding standard DRT image (right), at 8 GHz.

When longer CPIs are used with the standard DRT algorithms, image blurring occurs. Suppose κ as defined by (16) is set to 6, the Doppler resolution in the spectrogram of the signal becomes higher, as shown in Figure 7. When the corresponding cross-range profiles (with Doppler bin migration effects present) are applied to standard DRT, the resulting image is in Figure 8.

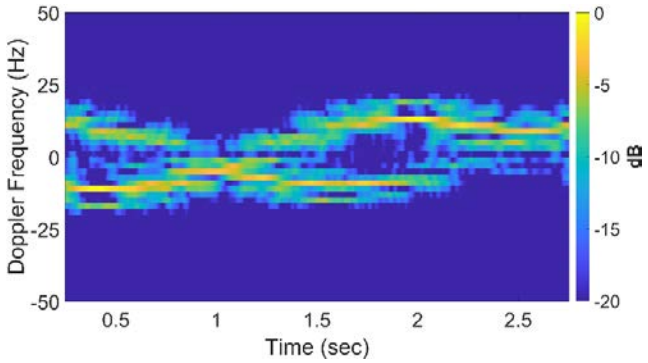

Figure 7: Signal spectrogram with augmented CPIs, augmentation factor of 6, at 8 GHz.

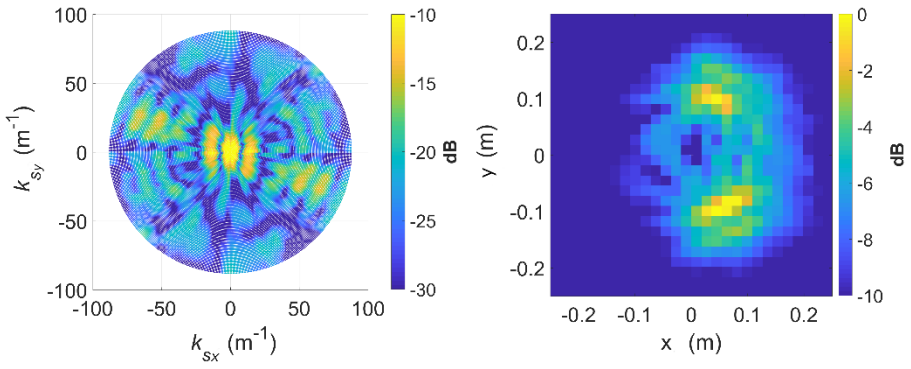

Figure 8: *k*-space support (left) and standard DRT image (right) with augmentation factor of 6, at 8 GHz

For a better insight into the electromagnetic scattering effects in this experiment, similar results using the highest frequency (12 GHz) available are shown in Figures 9 and 10. From Figures 7 and 9 it becomes

reasonably clear that in addition to direct (specular) scattering off the inner side of a metallic rod, creeping waves [13] around the rods are the most likely cause of the twin sinusoidal traces for each of the rods. The effects are clearly more pronounced at the shorter wavelength of 2.5 cm, which is more comparable to the rod diameter of approximately 2 cm. The double scattering effects are reflected in the 'shadowed blobs' in the DRT image.

Note that image blurring in standard DRT imaging due to long CPIs occurs only in the azimuthal direction; image focusing is still generally achieved in the radial direction.

4.4 Augmented DRT Imaging with OMP

To apply OMP for image focusing, the dictionary $\boldsymbol{\Psi}$ is set up with chirp atoms as defined in (18) and (19). Cross range *x* and range *y* are discretized over the interval $(-0.4, 0.4)$ m, with a nominal spacing of $\lambda/2$. As for the standard DRT demonstration, the two frequencies of 8 GHz ($\lambda = 3.75$ cm) and 12 GHz ($\lambda = 2.5$ cm) are used. Over the selected discretization interval, the number N_σ of atoms is thus 1849 (for 8 GHz) or 4096 (for 12 GHz).

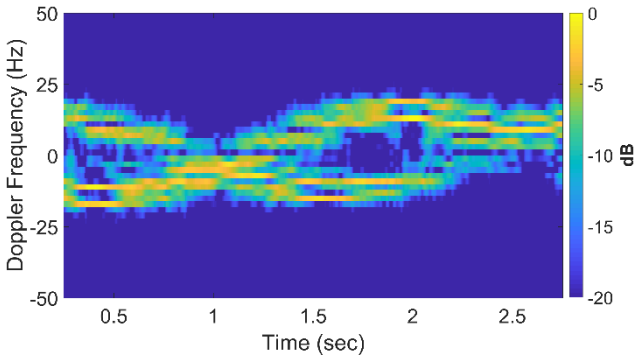

Figure 9: Signal spectrogram with augmented CPIs, augmentation factor of 6, at 12 GHz.

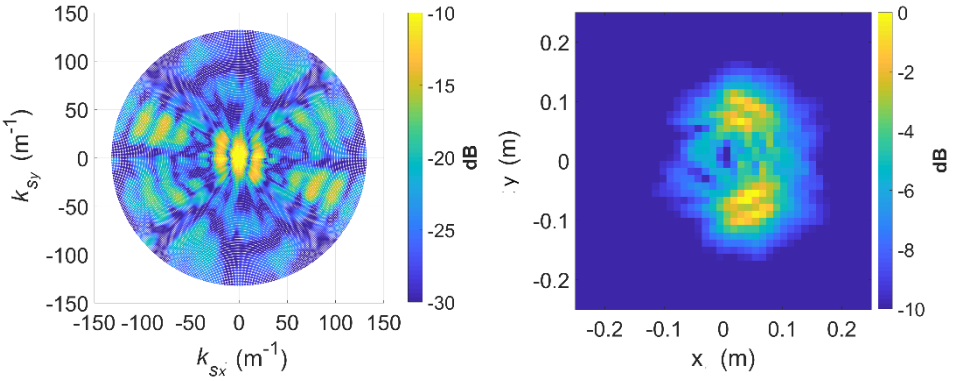

Figure 10: k-space support (left) and standard DRT image (right) with augmentation factor of 6, at 12 GHz

The coefficient magnitude of the first 20 atoms extracted from the 8 GHz signal show a clear convergence, as shown in Figure 11. The spectrogram of the reconstructed and `compressed' signal is shown in Figure 12 which clearly shows more resolvable sinusoidal traces compared to Figure 7.

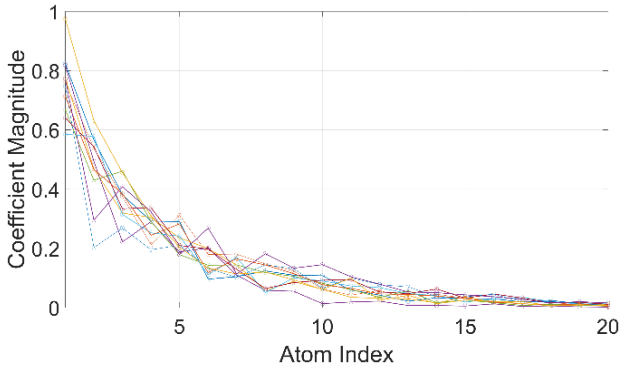

Figure 11: Magnitude of atom coefficients for first 20 atoms, shown for one in every 50 CPIs in the spectrogram, at 8 GHz.

To reduce signal processing noise effects in the resulting image, a simple thresholding method can be used to control the number atoms to keep in the sparse representation: in each CPI, stop the OMP iteration when atom coefficient magnitude falls below 20% of the maximum magnitude, as an example. This criterion can also save on computational cost, as less atoms need to be extracted in the processing. An example is shown in Figure 13 for the 8 GHz signal. Compared to Figure 8, this is a clearly significantly more focused image.

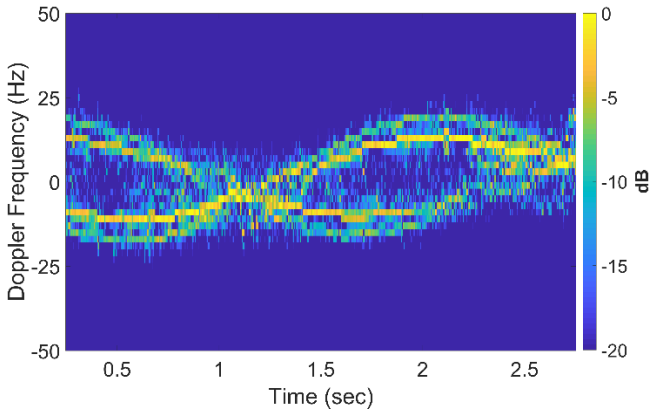

Figure 12: Spectrogram of reconstructed and OMP-focused signal with 20 atoms, at 8 GHz (compared to Fig.7)

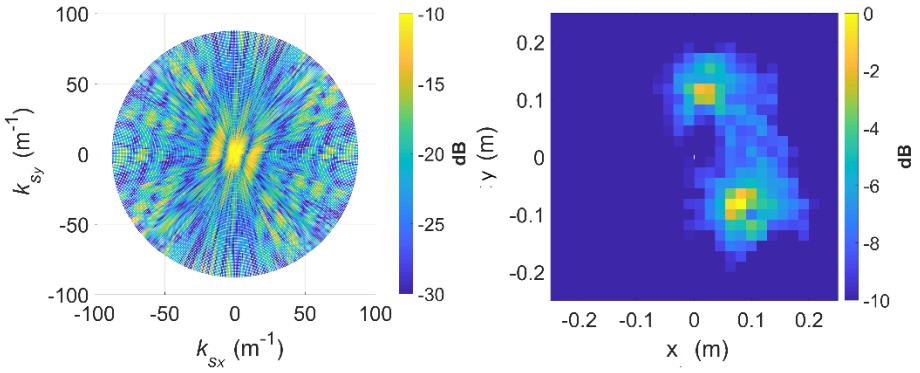

Figure 13: *k*-space support (left) and OMP-focused image (right) using a 20 % coefficient magnitude threshold, 8 GHz

For completeness, we also show results Figure 14 for the 12 GHz signal, which also resolve the scatterers significantly better using the OMP processing as compared to Figure 10 for standard DRT. The double scattering effects resulting in the 'double blobs' are also enhanced.

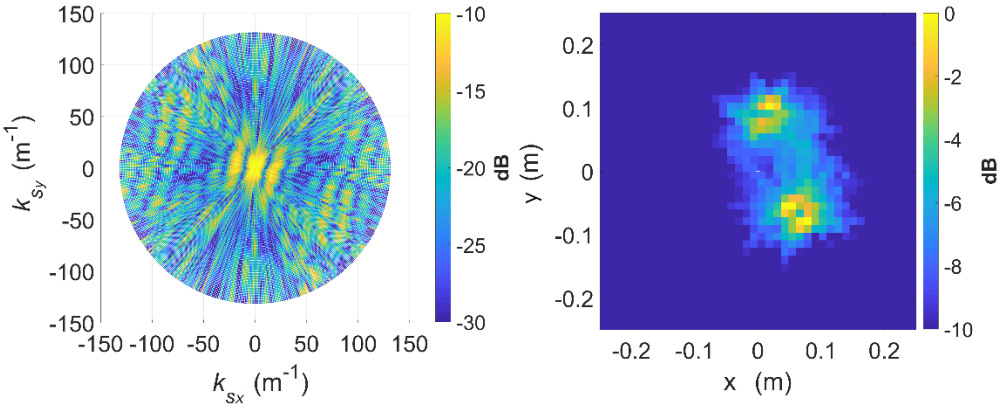

Figure 14: k-space support (left) and OMP-focused image (right) using a 20 % coefficient magnitude threshold, 12 GHz

4.5 The Off-Grid Problem in Target Imaging Based on Sparse Reconstruction

In the above demonstration, the spatial space (x, y) is discretized over rather arbitrary windows, with a nominal spacing of half a radar wavelength, creating a discrete grid from which to form the dictionary $\boldsymbol{\Psi}$. A major problem with this approach is a most likely certain mismatch with real target scatterers, which are not ideal point scatterers and may be located anywhere in a given volume of space. Even in the 2D approximation, real scattering centres may not fall exactly on any point of the dictionary grid. This results in the formation of multiple atoms with various coefficients, which can be expected to be in the neighbourhood of the real scatterer and whose linear sum approximate the real signal. In terms of image focusing, the formation may lead to noisy or blurry effects.

The problem has been discussed by several authors, such as in [14,15], in terms of basis mismatch. More recently a couple of methods have been proposed directly for the application of target imaging. The first method reported in [16] is a post-processing exploiting the tendency of atoms to cluster around true scatterers. The second method in [17], called Parameter-Refined OMP (PROMP), proposes an improved version of the OMP by replacing the linear least square step in its algorithm with a nonlinear least square

processing. Demonstrations using these methods on real experimental data is however beyond the scope of the current paper.

6.0 CONCLUDING REMARKS

We have demonstrated with experimental data that high-resolution imaging of a rotating target using an ultra-narrowband radar is possible. The enabling signal processing technique is a combination of Doppler radar tomography and a sparse reconstruction technique such as OMP, while a unifying mathematical framework is based on the slow-time *k*-space.

Acknowledgment: We sincerely thank Lorenzo Lo Monte and Nihad Alfaisali, and the Mumma Laboratory at University of Dayton, Ohio, USA, for collecting and providing the experimental radar data in May 2016.

REFERENCES

[1] Kak A.C. and Slaney, "Principles of Computerized Tomographic Imaging", Society of Industrial and Applied Mathematics, 2001.

[2] Tran H.T. and Melino R. "The Slow-Time k-Space of Radar Tomography and Applications to High-Resolution Target Imaging", IEEE Trans on Aerospace and Electronics Systems, vol.54, no.6, pp.3047-59, Dec 2018.

[3] Chen V.C. and Martorella M., "Inverse Synthetic Aperture Radar", Scitech Publishing, 2014, and references therein.

[4] Walker J.L., "Range-Doppler Imaging of Rotating Objects", IEEE Trans on Aerospace and Electronics Systems, vol.AES-16, no.1, 1980, pp.23-52.

[5] Ausherman D.A., Kozma A., Walker J.L., Jones H.M., and Poggio E.C., "Developments in Radar Imaging", IEEE Trans on Aerospace and Electronics Systems, vol.AES-20, no.4, 1984, pp.363-400.

[6] Jakowatz C.V., Wahl D.E., Eichel P.H., Ghiglia D.C., and Thompson P.A., "Spotlight-Mode Synthetic Aperture Radar: A Signal Processing Approach", Springer, 1996.

[7] Jakowatz C.V., Wahl D.E., Eichel P.H., Ghiglia D.C., and Thompson P.A., "Spotlight-Mode Synthetic Aperture Radar: A Signal Processing Approach", Springer, 1996.

[8] Soumekh M.,"Reconnaissance with Slant Plane Circular SAR Imaging", IEEE Trans on Image Processing, vol.5, no.8, pp.1252-65, Aug 1996.

[9] Mensa D., "Coherent Doppler tomography for microwave imaging", IEEE Transaction, Vol.71, no.2 June 1983.

[10] Tran H.T., and Melino R., "Application of the fractional Fourier transform and S-Method in Doppler radar tomography", Research Report, DSTO–RR–0357, DSTO, 2010.

[11] H.T. Tran, E. Heading, and B.-H. Ng, "On the Slow-Time k-Space and its Augmentation in Doppler Radar Tomography", IEEE Trans on Aerospace and Electronics Systems, (in review).

[12] Elad M., "Sparse and Redundant Representations: From Theory to Applications in Signal and Image

Processing", Springer, 2010.

[13] Knott, Eugene F & Shaeffer, John F & Tuley, Michael T (1993). "Radar Cross Section" (2nd ed). Artech House, Ch3, pp 83-84

[14] Herman, M.A.; Strohmer, T. "General deviants: An analysis of perturbations in compressed sensing". IEEE J. Sel. Top. Signal Process. 2010, 4, 342–349, doi:10.1109/JSTSP.2009.2039170.

[15] Chi, Y.; Scharf, L.L.; Pezeshki, A.; Calderbank, A.R. "Sensitivity to basis mismatch in compressed sensing", IEEE Trans. Signal Process. 2011, 59, 2182–2195, doi:10.1109/TSP.2011.2112650.

[16] N.H. Nguyen, K. Dogancay, H.T. Tran, and P. Berry, "An Image Focusing Method for Sparsity-Driven Radar Imaging of Rotating Targets", Sensors, 2018

[17] N.H. Nguyen, K. Dogancay, H.T. Tran, & P. Berry, "Parameter-Refined OMP for Compressive Radar Imaging of Rotating Targets", IEEE Trans on Aerospace and Electronics Systems, 2019 (in press)